Materials Science & Engineering A 556 (2012) 617–624

Contents lists available at SciVerse ScienceDirect

Materials Science & Engineering A

journal homepage: www.elsevier.com/locate/msea

Tensile deformation behavior of Ti–22Al–25Nb alloy at elevated temperatures

Peng Lin, Zhubin He, Shijian Yuan*, Jun Shen

School of Materials Science and Engineering, Harbin Institute of Technology, Harbin 150001, China

ARTICLE INFO

Article history:
Received 10 June 2012
Accepted 9 July 2012
Available online 25 July 2012

Keywords:
Ti_2AlNb
Deformation behavior
Strain rate hardening
Softening mechanism
Dynamic recovery

ABSTRACT

The deformation behavior of Ti–22Al–25Nb alloy at elevated temperatures and different stain rates was investigated using uniaxial tensile test. It was found that the tension was accompanied with the effect of hardening and softening, under which the stress–strain curve was characterized by a rise to a peak followed by a nearly linear drop in flow stress. The peak stress was strongly dependent on the temperature and strain rate. The underlying mechanism was clarified in terms of dislocation dynamics. Work hardening and strain rate hardening both contributed to the hardening mechanism, and the softening mode was dominated by dynamic recovery. The effect of work hardening was completely neutralized by dynamic recovery. Owing to the strain rate hardening, the alloy exhibited certain degree of superplasticity. The further drop in flow stress after the peak was due to the rise in temperature, which originated from the heat generated during deformation. The deformation mechanism was dominated by dislocation slip and climb. The misorientation distribution between β/B2 and α_2 phase scarcely changed, implying a harmonious deformation of the two phases.

1. Introduction

Ever since the ordered orthorhombic Ti_2AlNb (O) phase was discovered by Banerjee et al. [1], titanium aluminides with compositions based around the stoichiometry Ti_2AlNb have received considerable attention as potential high temperature structural materials. It has been shown that Ti_2AlNb-based alloys exhibit improved room temperature ductility, tensile strength and fracture toughness compared to the conventional intermetallic alloys such as TiAl-based and Ti_3Al-based alloys [2]. A Ti_2AlNb based alloy with the composition of Ti–22Al–25Nb (at.%) is an important member of this alloy group, which has been proved to have good mechanical properties at room and elevated temperatures [3].

Efforts on the development of Ti_2AlNb-based alloys to date mainly focused on composition design [4], thermal–mechanical processing such as forging and rolling operations on ingots [5], phase equilibrium and transformation [6], mechanical properties [7,8] and so on, which has significantly promoted the application progress of these alloys.

For industry applications, the Ti_2AlNb-based alloys finally have to be formed into desired shapes. Due to their limited ductility at room temperature, it is desired to form them at high temperatures. In general, the forming temperature ranges from 950 to 1000 °C [9], which is in the (α_2+O+B2) or (α_2+B2) phase field for most Ti_2AlNb-based alloys [10]. After forming, the workpiece subsequently has to be aged in the (O+B2) phase field to generate the desired microstructure and property, which is closely related to the previous forming processes. Therefore, to formulate the forming process regularly, a systematic investigation on the deformation behavior of Ti_2AlNb-based alloys at elevated temperatures is of significant importance. Up to now, investigations in this field have not been well documented.

The purpose of this study is to investigate the deformation behavior of Ti–22Al–25Nb alloy at elevated temperatures and different strain rates. To clarify the deformation mechanism, the microstructure and texture evolution during the deformation are examined as well. This work can be utilized as a guideline to control the forming process of this alloy group.

2. Experimental

The as-received material is a hot-rolled alloy sheet (1.25 mm thick) with a nominal composition of Ti–22Al–25Nb (at.%). The final rolling temperature is 940 °C. After hot-rolling, the alloy was subjected to 2 h annealing at 1000 °C followed by furnace cooling. The deformation behavior of the alloy was investigated by uniaxial tensile tests performed on an Instron 1361 machine attached with a high temperature furnace. The testing temperatures ranged from

* Corresponding author. Tel./fax: +86 451 86418776.
E-mail addresses: hithe@hit.edu.cn (Z.B. He), syuan@hit.edu.cn (S. Yuan).

0921-5093/$ - see front matter © 2012 Elsevier B.V. All rights reserved.
http://dx.doi.org/10.1016/j.msea.2012.07.036

930 to 990 °C at intervals of 20 °C and the initial strain rate settings were 1.00×10^{-2}, 3.16×10^{-3}, 1.00×10^{-3} and $3.16\times10^{-4}\,s^{-1}$. The tensile specimens were prepared along rolling direction, with a gage length of 10 mm and a width of 3 mm. To minimize oxidation, the gage section of each specimen was coated with glass slurry. To preserve the microstructure under testing temperature conditions, the specimens were rapidly water quenched. To investigate the deformation mechanism, the microstructure and texture of the initial and tensioned samples were characterized with scanning electron microscope (SEM) and electron backscattered diffraction (EBSD) techniques on Quanta 200 FEG-SEM machine. EBSD analysis was carried out with the help of software TSL OIM 5.31. The specimens for SEM and EBSD were prepared by electrochemical polishing with a solution of 6% perchloric acid, 34% butarol and 60% carbinol at 45 V and −40 °C. The EBSD data was collected with a step size of 1.0 μm. From the EBSD data, the phase map, inverse pole figure (IPF) plus image quality (IQ) map, pole figure (PF) and misorientation chart were calculated.

The phase map depicts the phase distribution of the alloy. The IPF shows the microstructure (including grain boundaries) and orientation distribution. The IQ is proportional to the sharpness of the Kikuchi Pattern, which is related to the presence of crystalline defects. A lattice distorted by crystalline defects such as dislocations and sub-grain boundaries will have a distorted Kikuchi Pattern, leading to a lower IQ value [11]. Therefore, the IQ can be utilized for the estimation of deformation, recovery or recrystallization degree [12]. The concrete texture components can be derived from the PF. The misorientation chart depicts the statistical distribution of misorientations between adjacent grains.

3. Results

3.1. Microstructure and texture of the as-received sheet

Fig. 1 shows the microstructure and texture of the as-received sheet that underwent 2 h annealing at 1000 °C after the final step of rolling. According to Ti–22Al–*x*Nb ternary phase diagram [10], the annealing temperature was in the ($\alpha_2+\beta$/B2+O) phase field but near the ($\alpha_2+\beta$/B2) transition line. According to the phase map (Fig. 1(b)), the principal phases of the sheet are β/B2 phase and the primary α_2 phase, as also shown in Fig. 1(a). The β/B2 phase exists in the form of matrix without obvious grain boundaries. The α_2 phase shows equiaxed shape embedded homogeneously in the β/B2 matrix.

Fig. 1(c) depicts the IPF plus IQ map calculated from the EBSD data. The β/B2 matrix is filled with a high density of low angle grain boundaries (LAGBs, $<15°$), which resulted from the movement and rearrangement of dislocations [13], suggesting that defects formed during the hot-rolling were not thoroughly eliminated by the annealing treatment. The orientation gradient of β/B2 matrix varied moderately and there are no obvious grains isolated by high angle grain boundaries (HAGBs, $\geq15°$), implying a sharp texture component, as depicted with PF in Fig. 1(d). The component can be represented with Miller index as $001\langle1\bar{1}0\rangle$ or with Euler angles as ($\varphi1=0°$, $\Phi=0°$, $\varphi2=45°$), which is one of the typical rolling textures along the α-fiber in BCC metals [14]. Most of α_2 phase grains are shown in green in Fig. 1(c), displaying an obvious texture as well. The component is marked with circles in Fig. 1(e) and can be represented as $11\bar{2}0\langle1\bar{1}00\rangle$ or ($\varphi_1=0°$, $\Phi=90°$, $\varphi_2=30°$). In addition, the α_2 phase also exhibits another

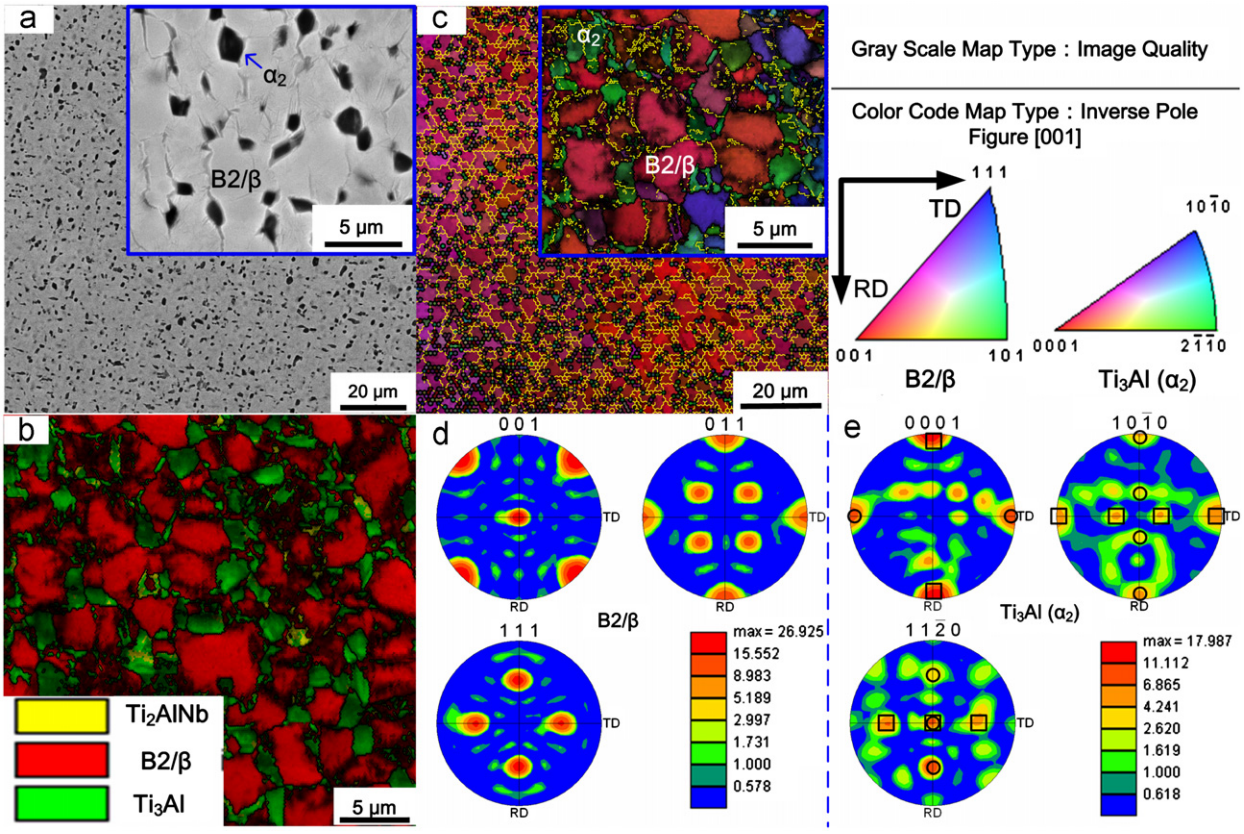

Fig. 1. Microstructure and texture of the as-received sheet: (a) SEM image, (b) phase map, (c) IPF+IQ map with high angle grain boundaries (HAGBs, ≧15°) shown in black and low angle grain boundaries (LAGBs < 15°) shown in yellow, (d) and (e) PF of B2/β phase and α_2 phase, respectively. (For interpretation of the references to color in this figure legend, the reader is referred to the web version of this article.)